

SIMULTANEOUS 3D-FLOW FIELD AND COMPLIANT WALL MEASUREMENTS IN A ABDOMINAL AORTIC ANEURYSM FLOW USING SCANNING-PTV

K. Hoyer *, M. Holzner, M. Guala, W. Kinzelbach

IfU, Dept. BAUG, 8093 Zürich, Switzerland - (hoyer, holzner, guala, kinzelbach)@ifu.baug.ethz.ch

KEY WORDS: index matching, scanning particle tracking velocimetry, flow phantom

ABSTRACT:

We combine well established particle tracking with wall surface measurements using tomographic scanning and present results for the non-stationary 4D - flow field within an abdominal aortic aneurysm (AAA) phantom. It was manufactured from an optically homogeneous but slightly opaque silicone having an index of refraction $n = 1.414$. The fluid used is a mixture of water and glycerol to match the index of refraction of the silicone to render the region of interest undistorted. The 3D data is acquired by means of rapidly scanning a laser sheet through the region of interest while simultaneously recording an image sequence of tracer particles using a single high speed camera. We mimic a symmetric quadruple camera setup by splitting the image 4-way using a custom made primary splitter in combination with four secondary adjustable mirrors. In addition to the seeded particles, which we identify and track in time, the aneurism wall lights up across the cut with the laser plane. In addition to the particle tracking, we will now also extract the surface of the moving interior wall through proper epipolar constraints, e.g. their intersection with a filtered edge detection map.

Previous measurements and attempts of different groups (MRI, DNS) to unify the stationary flow field data have shown the necessity to obtain the compliant wall motion simultaneously with the flow field boundary conditions. This paper addresses this issue to meet all necessary requirements that will allow further development of a numerical simulation tool.

1. INTRODUCTION

1.1 Motivation

The quantitative analysis and modelling of fluid flow in humans has become an increasingly important tool for decision making regarding e.g. the course of action for treatment. In patients with an aortic aneurysm, the risks of surgery have to be weighted against the risks of rupture. To date, the main decision criterion for or against surgical intervention is a critical aneurysm diameter of $D = 5$ cm.

Whereas this criterion is an empirically found result that should save most peoples lives with a diagnosed aneurism, each case exhibits its own flow topology. Additional fluid stresses on the arterial walls stem from flow redirection, flow separation and possibly wall attached vortex cores. Generally these additional stresses generate within the aneurism due to the sudden expansion and therefore act primarily on the arterial wall cells that have already weakened considerably. The very local nature of these repetitive alternating fluid flow stresses may contribute significantly to ones individual risk especially when the wall has lost enough elasticity and support tissue to actually collapse locally during the low pressure phase.

The final goal of this cooperative effort is to have a reliable numerical simulation tool that obtains the moving geometry and time dependent fluxes from individual patient MRI data to help in the decision process.

1.2 Aims

We aim to provide a complete experimental data set that allows the necessary verification and optimization of a numerical flow simulation, given the fluctuating wall surface and flux or pressure boundary conditions at the inlet and exits. Although the phantom geometry is modelled after an individual patient, the experimental setup will not simulate the exact flow in the patient mainly due to differences in the outlet impedances and the differences in the structural support. Nevertheless it will provide a viable data set, being a regular solution of the Navier-Stokes equations under the given boundary conditions.

Previous work using index matched liquids for optical flow measurements in complex geometries were pioneered by Edwards and Dybbs, 1984 (LDA in rod bundles) and later expanded by Hopkins et. al. 2000 (PIV in a nasal cavity). Here additionally we allow compliant wall motion compared to the previous investigations.

2. MATERIAL AND METHODS

2.1 Index matching

The AAA wall material is a permanently cured but flexible silicone from DOW Chemicals and was manufactured by repeatedly brushing the surface of a $\lambda = 3/2$ scaled up wax positive and curing the layer to the elastic state from the initially viscous liquid state. During the liquid state of the curing process, the positive wax geometry has to be constantly

* Corresponding author.

tumbled around in a specially designed rotating fixture to avoid large irregularities in the wall thickness.

The material exhibits a homogeneous index of refraction that has been matched using an approximate (40:60) mixture of glycerol and water. During the mixing and matching, the refractive index of the solution was repeatedly measured using a Bellingham + Stanley Eclipse 45-41 refractometer, which allowed approaching the ideal mixture asymptotically.

2.2 Particles

As tracer particles we added Rhodamine labelled particles with a nominal size distribution of $64 \mu\text{m} < d_{90} < 128 \mu\text{m}$. It was necessary to use labelled particles to increase the signal to noise ratio of the particle signal. Unfortunately, the silicone material was more opaque than it should ideally have been. Although a certain opaqueness is desirable, too much scatter from the wall increases the background grey value and also blocks light especially to regions where it has to pass multiple wall segments.

2.3 Scanning laser sheet

Our laser sheet is obtained by expanding an Ar-Ion laser beam of approximately 2.5 mm diameter using a cylindrical lens. The sheet thickness at the observation volume adjusts to approximately $d_{LS} = 1 \text{ mm}$ using a long focal length cylindrical lens. The so generated laser sheet then passes through a rotating 8-face-parallel cylindrical prism ($n_p=1.49$) that scans the transmitted light across a distance $s = 45 \text{ mm}$. The scanning laser sheet then is mirrored directly to the region of interest such that the light passes through the model in the least self obstructing way, possibly compromising the ideal case of the scan direction be as aligned to the camera axis as possible to maximize data yield.

2.4 Camera setup and image splitter

We use a single Photron Ultima APX highspeed camera ($1\text{k}^2 @ 17.5 \mu\text{m}$ square pixels) with Nikkor 25 mm focal length lens set at f#22 to maximize depth of field. Additionally a yellow filter (Nikon Y52) reduced the direct scatter of the laser light and passed the Rhodamine emitted light essentially unhindered. This allowed additional signal improvement for the fluid phase tracking. Alternatively the future data will be acquired using a single line of the Ar-Ion laser. The additional spectral separation from the 488 nm line to the Rhodamine emission may still improve the SN-ratio.

The camera chip receives four projected images via an image splitter exhibiting precision bevelled front coated mirrors to minimize imager area loss. Four secondary mirrors allow precise image alignment using adjustable pan/tilt fixtures.

3. DATA ACQUISITION AND PROCESSING

3.1 Camera calibration

The camera calibration is achieved using a standard PIV target positioned at two known planes separated approximately as to border the front and back of the region of interest with respect to the camera axis. The back calibration image was taken through the AAA phantom. This image was high pass filtered after which edge artefacts from the phantom were removed,

whereas the front calibration image in front of the phantom. To give an impression for the index match quality we show the original back calibration image in figure 1.

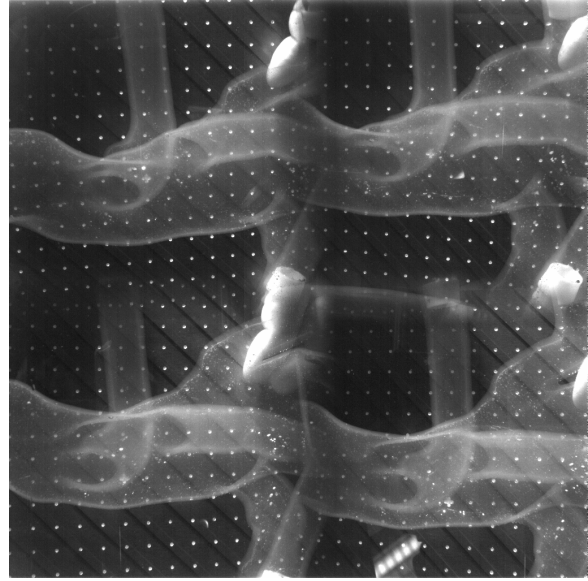


Figure 1. Raw back plane calibration image as seen through the image splitter. In the foreground one recognizes the slightly opaque AAA phantom (upper arterial branches)

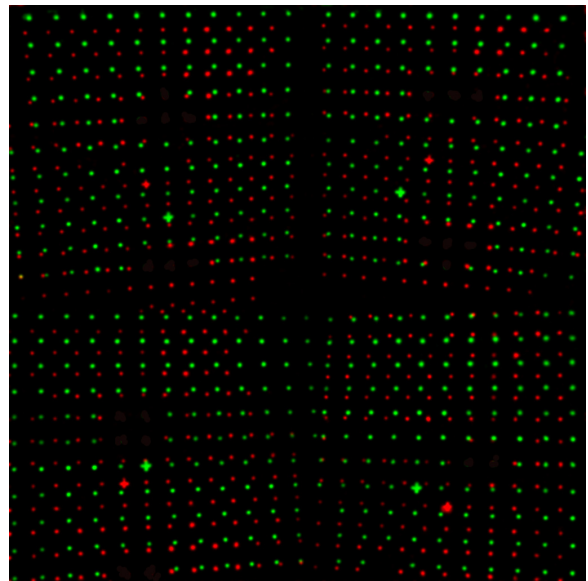


Figure 2. Cleaned and combined front/back (green/red) calibration image used for the calibration.

Together with a target file of the “true” 3D coordinates, this image file allows determination of the inner and outer camera parameters with respect to a chosen coordinate system. The calibration, the particle recognition and the stereoscopic matching through the multimedia geometry is detailed in Maas (1992). The calibration of the camera model allowed identification and stereo-matching of about 400 particles per slice. The positioning accuracy is about $50 \mu\text{m}$ in the normal to and about $300 \mu\text{m}$ parallel to the camera axis. The decreased resolution along the optical axis can be explained with the large working distance when imaging a relatively large region of interest using the 4 way splitter geometry and a 25 mm focal

length lens. A shorter focal length lens may also help to improve this compromise.

3.2 Camera trigger

The camera is being triggered in “random reset“-mode which allows exact synchronization to the rotating prism or each new start of the laser scan. On the trigger, the camera timer is reset after which a set number of images are taken at a pre-programmed frame rate. In our case we obtained 20 images at 2 kHz camera frame rate per trigger. This requires that the volume scan rate is less than 100 Hz for the camera to finish acquiring before the next trigger comes. In our case, the volume scan rate was set to a safe value of 94.5 Hz

3.3 Image sequence

In SPTV we use a laser sheet that scans perpendicular to its plane, whereas a camera repeatedly takes a rapid image sequence. To illustrate the process, we have added a filmstrip image of a volume scan through the region of interest

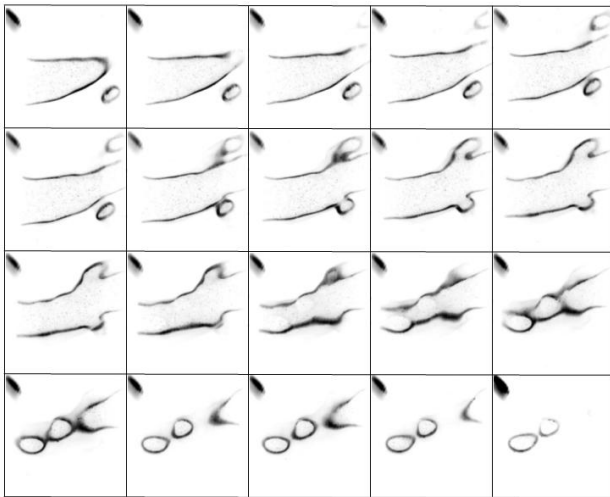


Figure 3: Filmstrip of one volume scan through the aorta as imaged by one camera view. Time progresses from left to right and from top to bottom. The camera frame rate is 2 kHz and is acquired within 1/100 s.

As a result of the fast sequential image acquisition we have an observation volume that is gathered with increasing time stamp, e.g. the far planes are scanned after the near planes. For the tracking and post-processing it is desirable to have all data interpolated to a single time stamp for each volume scan. The detailed code adaptations for SPTV post-processing have been published recently Hoyer et al. (2005). We tracked the particle data sequence using a correlation based approach detailed in Hoyer et al. (2006). For now, we will focus on the edge detection algorithm used to determine the wall coordinates. Figure 4 shows a single slice of raw data of the top/left 512² pixels, where seed particles and aortic wall are visible being illuminated by a thin slice. The edge detected by the image pre-processing is also highlighted a red pointed line. We can see that the obstruction of the illuminated region by dark wall material leads to false edges, visible in edge detected the lower right artery. Since these false edges do not generally result in matched edges, they do not show up in the result. Only edges that have stereoscopic matches are determined real, data that does not result in stereoscopic matches is discarded.

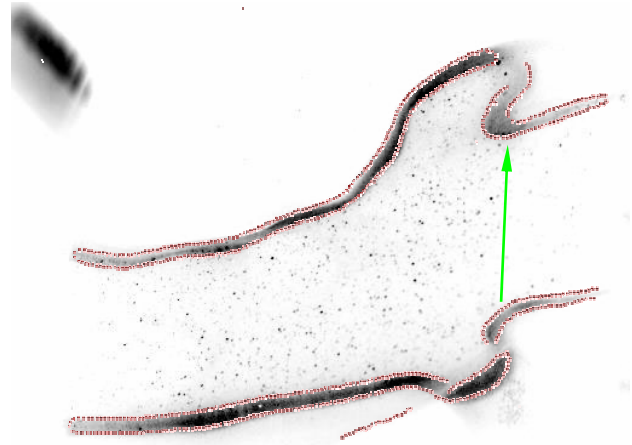


Figure 4. Top/left quarter of the imager chip with typical raw data (grey) and pearl-string contour (red). The green arrow is parallel to the laser light. Both the illumination and the observation paths are partly obscured by wall material; especially noticeable as dark region (top right) and as edge artefact through the lower segment (bottom right), respectively.

The scanning laser sheet adds an additional dynamic thickness to the width of the laser sheet. When scanning the sheet perpendicular to its plane, the illuminated region grows linearly with time. To obtain a sharp contour it is therefore desirable to have a thin static sheet and a short exposure time. Since the particle recognition requires the shutter to be open for the inverse of the frame rate, we can only increase the frame rate to minimize this dynamic effect. For the surface extraction, the images were pre-processed to remove the particles and to increase the signal from the wall scatter using low pass filtering and gamma correction. The edge detection and segmentation was achieved using the LabView image processing toolbox.

3.4 Surface extraction

The surface extraction is achieved by processing the edge segments as strings of particles. Therefore we generated finely discretized lines of “particles” along all edge sequences to feed to the particle recognition and matching code. When the line is discretized in increments smaller than the tolerance to the epipolar line, the stereoscopic matching algorithm will find some candidates and chooses the match with the least error in every image as long as a common edge has been detected. The additional noise introduced to the wall coordinate is directly related to the discretization and thus can be reduced to levels comparable with regular particle recognition uncertainties. For the current application, memory or processing time restraints have not surfaced using this approach.

Figure 5 shows the reconstructed volume obtained with the described edge detection displaying the main abdominal aortic branches supplying kidneys and digestive tract. The branch leading out to the bottom right exhibits decreased resolution and possibly artefacts due to the mentioned obstruction in the observation path. This obstruction can be reduced by processing also unambiguous stereo pairs. This is possible only when the location of the arbitrarily inclined scanning plane is modelled correctly in time, so that the epipolar lines can be kept as short as possible. This can be done in a second step after processing the images in a first step using little restriction on the length of the epipolar lines. The arbitrary inclination and scanning

direction is necessary to avoid obstruction of the illumination path. This iterative second step is not yet implemented and the particle cloud presented in Figure 5 was compiled from triplets and quadruplets, e.g. common points recognized in three and four cameras simultaneously, respectively. Possibly also other topological features such as the grey value gradient will be needed to sort out doublet match ambiguities from opposite surfaces.

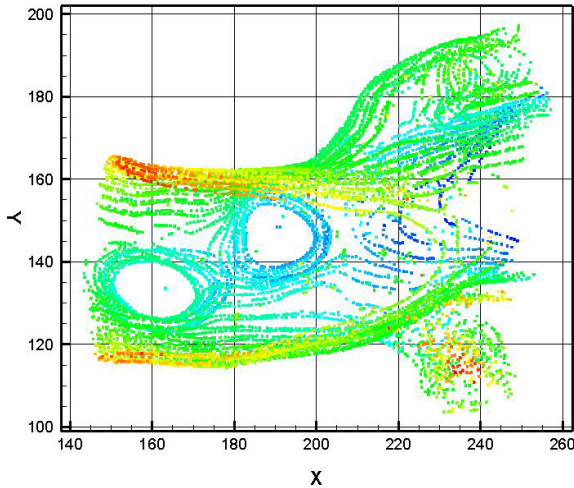


Figure 5. Inner and outer surface contours of the aortic wall compiled from 20 slices. Colours indicates Z-coordinate (red near /blue far) (units in [mm])

3.5 Flow field extraction

The flow field in the observed experiment has a mean velocity of $U = 0.23$ m/s which leads to a Reynolds number of $Re = 690$ based on the aorta diameter $D = 0.03$ m and kinematic viscosity of the water glycerol mixture $\nu = 10^{-5}$ m²/s. Scanned with a volume scan rate of 94.5 Hz, the average displacement of the particles per time step is over 2 mm, whereas the average separation between nearest neighbours is about half that distance. The fluorescing Rhodamine labelled particles were illuminated using the 514 nm line of the Ar-Ion laser.

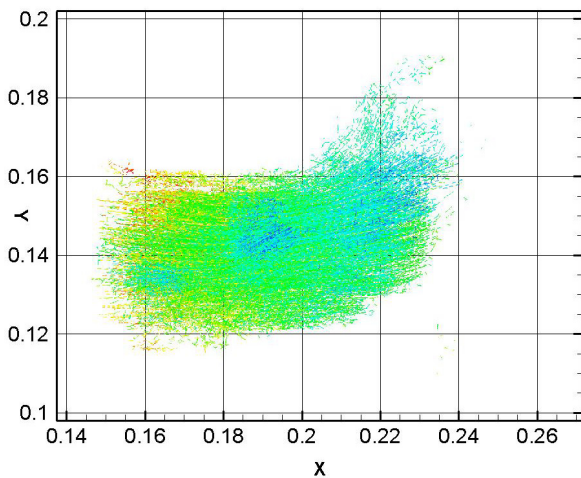


Figure 6: Tracked particle velocity vectors cumulated over 12 frames, encoded in like colours to compare with Figure 4. Data density is excellent within the aorta and where illumination and observation was not obstructed (units in [m])

We were also using a yellow filter to increase the signal to noise ratio for the particles, however had trouble recognizing particles in the darker regions, which is especially true at the Gaussian tails of the laser sheet intensity. Contrary to the image preprocessing for the wall surface, the particle images were high pass filtered and not gamma corrected. This results in reduced data density marking the flow into one of the arteries (top right). Again, the bottom right artery has even less data although the light intensity was higher here. This again is due to the common obstruction in the observation path through the tangential projection of the wall material.

4. CONCLUSION

We are presenting a highly resolved flow field within a replica of an abdominal aortic aneurysm using SPTV for the illumination of the tracer particles and the phantom wall. From a total of 11500 detected particles per volume scan, 4000 interpolated trajectories remained after tracking and trajectory interpolation. The scattered light from the opaqueness of the phantom wall material exceeds by far the signal from the particle images. Therefore we used spectral separation between the excitation at 514 nm and the particle Rhodamine emission using a yellow filter. The model wall was more opaque than necessary which resulted in reduced data quality and necessitated workarounds. The particle recognition and matching algorithm allows essentially an arbitrary orientation of the illuminating light sheet, which is necessary to optimize the light path through the model phantom with respect to the obstruction of the incoming light. Although optimally perpendicular to the common camera symmetry line, the direction and motion of the scanning sheet has to avoid also connection tubing and fittings within the model tank. The optical access of both illumination and observation has to be carefully judged before designing and building a generally customized glass-walled container. We present a single observation volume of only a part of the entire flow phantom. We plan to repeat and optimize the measurements over the entire phantom to obtain a dynamic flow field and wall motion map as an experimental baseline and boundary conditions to allow improvement of the direct numerical simulation of such flow problems.

4.1 References

- Edwards, R.V., Dybbs A., 1984, Refractive index matching for velocity measurements in complex geometries. *TSI Quarterly*, Volume X, Issue 4, Oct-Dec. 1984
- Hopkins, L. M., Kelly, J. T., Wexler A. S., Prasad, A.K., Particle image velocimetry in complex geometries. *Experiments in Fluids*, 29, 91-95, 2000
- Hoyer, K., Holzner, M., Lüthi, B., Guala, M., Liberzon, A., Kinzelbach, W., 3D Scanning particle tracking velocimetry. *Experiments in Fluids*, 39, 923-934, 2005
- Hoyer, K., Holzner, M., Kinzelbach W., Correlation based particle tracking Velocimetry, *5th International Symposium on Turbulence, Heat and Mass Transfer*, Dubrovnik, Croatia, September 25-29, 2006
- Maas, H.-G., Doctoral thesis: Digitale Photogrammetrie in der dreidimensionalen Strömungsmesstechnik, Dissertation ETH Nr.: 9665, 1992.

4.2 Acknowledgements

We wish to express our gratitude to the Swiss national science foundations CO-ME program sponsored through the National Centres of Competence in Research (NCCR).